Computational Characterization of Aerosol Delivery for Preterm Infants

I. Aramendia, U. Fernandez-Gamiz, A. Lopez-Arraiza, M. A. Gomez-Solaetxe, J. M. Lopez-Guede, J. Sancho, F. J. Basterretxea

Abstract— The aerosolization of perfluorocarbons along with non-invasive respiratory support has showed promising results as an alternative to treat the respiratory distress syndrome (RDS) in preterm infants. The aim of this study was to evaluate the main characteristics of the aerosol generated by an intracorporeal inhalation catheter, where one central lumen deliver the liquid and six peripheral lumens deliver the compressed air. Initially, different experiments were made with sterile water at different driving pressures to analyze properties such as the aerodynamic diameter (D_a), mass median aerodynamic diameter (MMAD) and geometric standard deviation (GSD). Subsequently, the perfluorocarbon FC-75 was tested to obtained experimental data to define the boundary conditions and to validate the numerical model. The experimental validation of the numerical model provided an accurate prediction of the air flow axial velocity and suggested that the collision and coalescence of the particles plays a crucial role in the particle size and mass distribution.

***Keywords*—**Aerosol, CFD, Inhalation catheter, Respiratory Distress Syndrome

I. Introduction

EXTREMELY and very preterm infants present cerebral and pulmonary issues due to the immaturity of the lungs, primarily caused by the lack of surfactant. This leads to the Respiratory Distress Syndrome (RDS) of the newborn, which is the leading cause of death in premature babies. [1]. This natural substance covers the alveoli, being its main goal to reduce the surface tension and, therefore, to prevent alveolar collapse at the end of the exhalation, retaining enough air to start the next breath. The current surfactant replacement therapy implies some drawbacks, as the requirement of intubation and the application of ventilator support techniques, which can result in lung injury and chronic lung diseases (CLD) [2]-[3]. In this regard, the neonatologists are focused on new minimally invasive surfactant therapies (MIST) as an alternative to solve the current dilemma; how to deliver exogenous surfactant without invasive techniques when the application of continuous positive airway pressure (CPAP) is not enough [4]. The guidelines recommend nowadays the use of natural surfactants instead of synthetic ones and as early as possible in the course of RDS [5]. It is also reported a survival advantage with higher initial doses of natural surfactant (200 mg/kg better than 100 mg/kg using poractant alfa) and fewer requirement of a second dose [6].

One alternative therapy is the INSURE technique (Intubation, Surfactant, Extubation) firstly reported by Verder et al. [7] in 1994. It consists in intubating the preterm infant for surfactant administration with quick (within 10 minutes) extubation to nCPAP. Sandri et al. [8] published a randomized controlled trial to evaluate the efficacy of combining prophylactic surfactant and early selective surfactant, with nCPAP in preterm infants. Their results showed that prophylactic surfactant given within 30 minutes of birth was not superior to early selective surfactant in terms of requirement of MV in the first 5 days of life. The tracheal catheterization is the most extensively method studied so far. Dargaville et al. [9] developed the Hobart method, where Curosurf surfactant at a dose of 100 mg/kg is administered using a semi-rigid vascular catheter briefly passed into the trachea beyond the vocal cords. The results showed that surfactant can be effectively delivered by this technique with a considerably reduction of intubation and MV in the first 72 hours [10]. Currently, they are working on a randomized control trial (the OPTIMIST-A trial) evaluating a total of 606 infants which is expected to be completed in 2020 [11].

The administration of nebulized surfactant is a promising technique to treat lung diseases and especially RDS even though there are still technical issues and challenges to lead. Four clinical trials have been published [12-15] showing that

This work was supported by Consolidated Groups from the Basque Government.

I. Aramendia is with the University of the Basque Country UPV/EHU. He is now with the Nuclear Engineering and Fluid Mechanics Department, Vitoria-Gasteiz, Alava 01006 Spain (phone: 945014123; e-mail: inigo.aramendia@ehu.eus).

U. Fernandez-Gamiz is with the University of the Basque Country UPV/EHU. He is now with the Nuclear Engineering and Fluid Mechanics Department, Vitoria-Gasteiz, Alava 01006 Spain (e-mail: unai.fernandez@ehu.eus).

A. Lopez-Arraiza is with the University of the Basque Country UPV/EHU. He is now with the Department of Nautical Science and Marine Systems, Bilbao, Bizkaia 48013 Spain (e-mail: alberto.lopeza@ehu.eus).

M. A. Gomez-Solaetxe is with the University of the Basque Country UPV/EHU. He is now with the Department of Nautical Science and Marine Systems, Bilbao, Bizkaia 48013 Spain (e-mail: miguel.solaetxe@ehu.eus).

J. M. Lopez-Guede is with the University of the Basque Country UPV/EHU. He is now with the Systems Engineering and Automatics Department, Vitoria-Gasteiz, Alava 01006 Spain (e-mail: jm.lopez@ehu.eus).

J. Sancho is with the University of the Basque Country UPV/EHU. He is now with the Nuclear Engineering and Fluid Mechanics Department, Vitoria-Gasteiz, Alava 01006 Spain (e-mail: javier.sancho@ehu.eus).

F. J. Basterretxea is with the University of the Basque Country UPV/EHU. He is now with the Department of Physical Chemistry, Bilbao, Bizkaia 48013 Spain (e-mail: franciscojose.basterretxea@ehu.eus).

is a feasible and safe technique, however, only one of them [12] has demonstrated good results. Currently, Pillow and Minocchieri are working on a new clinical trial, the CureNeb study, where preterm infants receive either CPAP or CPAP and nebulized surfactant in the first 4 hours of life [16]. Another alternative is the use of perfluorocarbons (PFC) instead of surfactant. Burkhardt et al. [17] have demonstrated that is useful to improve surfactant distribution and that resulted in an improved oxygenation.

One of the main reasons of the low efficiency of nebulized surfactants in these clinical trials is the relative low lung deposition rates (less than 1% of the mass nebulized) with conventional jet and ultrasonic nebulizers [18, 19]. Nevertheless, Goikoetxea et al. [20] have studied the potential to deliver relatively large amounts of surfactants and perfluorocarbons beyond the third generation of branching in a neonatal airway model through an intracorporeal inhalation catheter (IC). The influence of four different ventilation strategies on surfactant and PFC aerosol production rate were studied in an *in vitro* study by Murgia et al. [21]. The results showed that higher peak inspiratory pressure (PIP) and higher respiratory rates (RR) might enhance surfactant and PFC delivery to the lungs but might also increase compound loss during expiratory phase. Syedain et al. [22] have introduced recently a novel device of narrow gauge (outside diameter < 1mm) to be inserted into an endotracheal tube that should allow intra-pulmonary aerosol generation and near complete drug delivery while maintaining low air pressure and flow.

Numerical models through Computational Fluid Dynamics (CFD) techniques provides a useful methodology to study the behavior of aerosol particles in the airways and to obtain valuable data related with airflow patterns, particle deposition and particle size distributions. Zhang et al. [23] have studied the influence of inlet velocity profile on a three generation bronchial airway of human lung model for eight Reynolds numbers ranging from 200 to 1600. Farkas et al. [24] have simulated the particle deposition patterns and deposition efficiencies in particle size ranges from 1 nm to 10 µm. On the other hand, Longest et al. have evaluated how geometry simplifications can significantly influence in terms of deposition. The use of a more realistic geometry model in comparison with a simplified one increased the deposition of ambient aerosols [25]. However, most of these CFD studies are focused on adult airways and the conclusions cannot be extrapolated on preterm infants' airways due to differences in dimensions and breathing conditions. Liu et al. [26] have simulated the deposition of particles from the mouth to the third generation of the airways in a model for a 3 year old child. They conclude that the airflow rate, particle diameters and particle density are three key factors affecting particle deposition rates for children. De Jongh et al. [27] made also a CFD deposition study with particles from 1 to 5 µm in the upper airway of a 9-month-old child. Goikoetxea et al. [28] evaluated with a numerical model the aerosol delivery of surfactant and perfluorodecalin (PFD) by means of an inhalation catheter (IC). The results showed the beneficial effects of generating an intracorporeal aerosol with minimal airway manipulation.

The structure of the paper starts with a description of the experimental setup used to generate aerosols with an inhalation catheter and the results obtained for sterile water and FC-75 respectively. Then the numerical model is introduced, defining the geometry, discretization, boundary conditions and the physics involved in its development. Finally the experimental validation of the numerical model is presented and the conclusions are discussed.

II. EXPERIMENTAL SETUP

Aerodynamic diameter is defined as the physical diameter of a unit density sphere that settles through the air with a velocity equal to that of the particle in question. It is the most significant aerosol size parameter because it determines the particle's behavior while airborne. Particles exhibiting the same airborne behavior have the same aerodynamic diameter, regardless of their physical size, shape, density or composition.

An Aerodynamic Particle Sizer (APS 3321, TSI Incorporated) has been used, which provides high-resolution, real-time aerodynamic measurements of particles from 0.5 to 20 µm. This spectrometer uses two partially overlapping laser beams to detect coincidence. Thus, as a particle passes through these overlapping beams it generates one signal with two crests, as shown in Fig. 1. The time between the crests, which is called time-of-flight, involves measuring the acceleration of aerosol particles, with larger particles accelerating more slowly due to increased inertia. Using polystyrene latex (PSL) sphere calibration, which is stored in non-volatile memory, the spectrometer converts each time-of-flight measurement to an aerodynamic particle diameter.

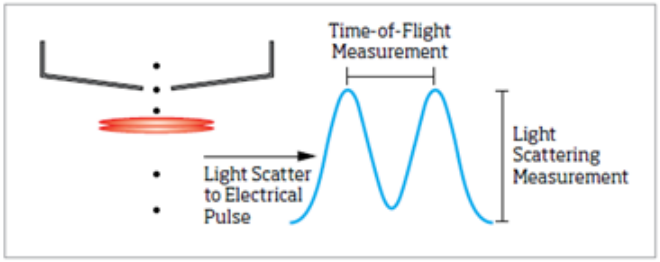

Fig.1 Double-Crested signal from particles passing through overlapping beams

An inhalation catheter (IC) (AeroProbe, Trudell Medical International), illustrated in Fig. 2, was used to produced the aerosol. Sterile water (H2Od, B. Braun Melsungen, Germany; density = 0.9982 g/ml; kinematic viscosity =1.003 cSt; surface tension = 0-30 dyne/cm) has been used to simulate the aerosolization at different driving pressures (4-6 bar). The compressed air is delivered through six peripheral lumens and the liquid is delivered through the central lumen. The close proximity of these lumens at the catheter tip results in efficient aerosolization of the liquid. Additionally, the perfluorocarbon (PFC) compound FC-75 ($C_8F_{16}O$, Fluorinert, 3M, Neuss, Germany; density = 1.78 g/ml; kinematic viscosity = 0.81 cSt; surface tension = 15 dyn/cm) has been tested. Different PFC have been previously used in several animal experiments with promising results [29].

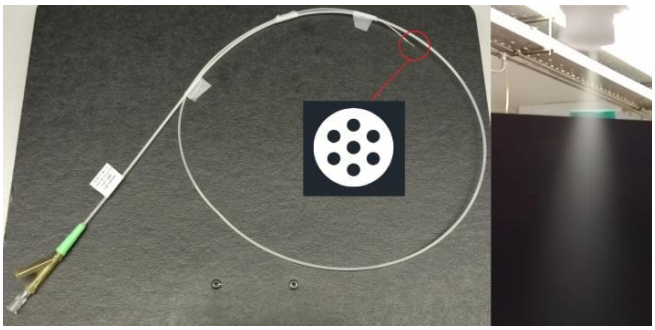

Fig. 2 Inhalation catheter IC 1.1

The IC has been connected to a pressure control system (ValveMate 7040, EFD Nordson Company), which allows to change the driving pressure between 0-7 bar. The scheme of Fig. 3 shows the equipment and experimental setup used to study the aerosol formation. The distal end of the IC has been aligned with the nozzle of the APS in order to obtain an accurate measurement of the aerosol generated and different distances between the distal end of the IC and the nozzle has been set to check the concentration of the aerosol. Even though the usable data of the APS is up to 10.000 particles/cm^3 the average recommended particle concentration is 1000 particles/cm^3. The spectrometer also clasify the particles in four different events or groups in order to control the measurement accuracy. To obtain reliable data it is necessary to have most of the sample data classified in the second event, which measures the particles between 0.5-20 µm. The other events classify the particles smaller than 0.5 µm, particles bigger than 20 µm and the particle coincidence, which occurs when more than one particle cross the laser beams at the same time. All the data and information captured by the APS is recorded and visualized by the Aerosol Instrument Manager (TSI) software.

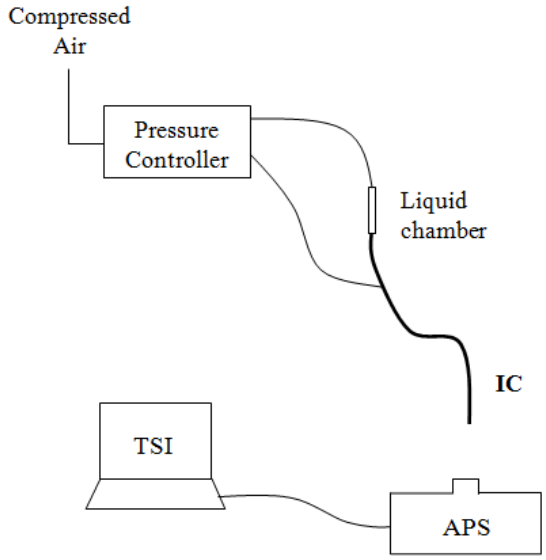

Fig. 3 Experimental set-up for the particle size characterization

III. EXPERIMENTAL RESULTS

Six different cases were studied with sterile water as can be seen in Tables I-VI varying the driving pressure and the distance between the distal end of the catheter and the nozzle of the APS where the measurements are taken. Five samples have been recorded for each case, with a sample time of 10 seconds. At first, it was necessary to establish the optimal distance between the catheter tip and the APS nozzle in order to obtain accurate measurements. As can be seen in Table 1, the initial distance for sterile water was set at 34.5 cm providing a concentration much higher than the recommended of 1000 particles/cm^3 in every sample. It was found that the optimal distance were 42 cm and 5.2 cm for the sterile water and the FC-75 respectively.

The geometric standard deviation (GSD), the mass median aerodynamic diameter (MMAD) and the aerodynamic diameter (Da) have been analyzed to study the particle size characterization. The GSD is a dimensionless number which gives an indication of the spread of sizes of particles that make up the aerosol. An aerosol is made up of particles of many different sizes (heterodisperse aerosol) with a GSD above 1.25. On the other hand, a GSD below 1.25 indicates that all the aerosol particles are of the same or very nearly the same size (monodisperse aerosol). The MMAD is defined as the value of the aerodynamic diameter (Da) such that half the mass of the aerosol is contained in small diameter particles and half in larger. The relationship between the aerodynamic particle diameter (Da) measured by the APS and the geometric particle diameter (Dg) is given by (1):

$$D_g = D_a \sqrt{\frac{\rho_0}{\rho}} \quad (1)$$

where ρ0 is the unit density (1 g/cm^3) and ρ the density of the compound to be nebulized, in this case sterile water (ρ =0.9982 g/cm^3).

Sample	Da (µm)	MMAD (µm)	GSD	Concentration (particles/cm^3)
1	2.64	9.59	2.16	1910
2	2.38	9.37	2.13	1740
3	2.98	9.64	2.25	1620
4	3.56	9.54	2.19	2150
5	3.39	9.65	2.24	1550
MEAN	**2.99**	**9.56**	**2.19**	
SD	**0.49**	**0.11**	**0.05**	

Table I. Pressure: 3.5 bar; Distance IC-APS: 34.5 cm

Sample	Da (µm)	MMAD (µm)	GSD	Concentration (particles/cm^3)
6	2.69	9.83	2.26	1430
7	3.72	9.62	2.17	1860
8	4.03	9.63	2.10	1880
9	4.14	9.97	2.14	1460
10	4.16	10.1	2.12	1230
MEAN	**3.75**	**9.83**	**2.16**	
SD	**0.62**	**0.21**	**0.06**	

Table II. Pressure: 4 bar; Distance IC-APS: 34.5 cm

Sample	Da (µm)	MMAD (µm)	GSD	Concentration (particles/cm^3)
16	4.00	10.3	2.20	1040
17	4.09	10.3	2.19	1210
18	4.08	10.1	2.15	1240
19	4.12	9.89	2.14	1060
20	4.01	10.2	2.21	1050
MEAN	**4.06**	**10.16**	**2.18**	
SD	**0.05**	**0.17**	**0.03**	

Table III. Pressure: 4 bar; Distance IC-APS: 42 cm

Sample	Da (µm)	MMAD (µm)	GSD	Concentration (particles/cm^3)
21	4.55	10.8	2.09	1020
22	4.24	10.2	2.14	879.8
23	4.33	10.6	2.16	780
24	4.51	10.5	2.06	965.3
25	4.67	10.9	2.08	917.9
MEAN	**4.46**	**10.60**	**2.11**	
SD	**0.17**	**0.27**	**0.04**	

Table IV. Pressure: 4.5 bar; Distance IC-APS: 42 cm

Sample	Da (µm)	MMAD (µm)	GSD	Concentration (particles/cm^3)
27	4.54	10.4	2.09	691.3
28	4.77	11.1	2.08	671.6
29	4.76	11	2.08	671.3
30	4.83	11.1	2.04	745.6
31	4.91	11.1	1.98	1090
MEAN	**4.76**	**10.94**	**2.05**	
SD	**0.14**	**0.30**	**0.05**	

Table V. Pressure: 5 bar; Distance IC-APS: 42 cm

Sample	Da (µm)	MMAD (µm)	GSD	Concentration (particles/cm^3)
35	4.79	11.1	2.00	1310
36	4.88	10.7	1.89	1420
37	4.86	10.5	1.86	1580
38	4.89	10.1	1.84	1650
39	4.79	10.4	1.87	1530
MEAN	**4.84**	**10.56**	**1.89**	
SD	**0.05**	**0.37**	**0.06**	

Table VI. Pressure: 6 bar; Distance IC-APS: 42 cm

The same procedure was carried out with the FC-75 compound with a driving pressure of 4 bar and its optimal distance (See Table VII). This data was used to validate the results of the numerical model.

Sample	Da (µm)	MMAD (µm)	GSD	Concentration (particles/cm^3)
1	2.47	10.5	1.70	1140
2	2.45	10.1	1.69	1160
3	2.44	10.3	1.70	1190
4	2.45	9.73	1.68	1210
5	2.43	9.42	1.68	1140
MEAN	**2.45**	**10.01**	**1.69**	
SD	**0.01**	**0.44**	**0.01**	

Table VII. Pressure: 4 bar; Distance IC-APS: 5.2 cm

Additionally, the particle size distribution was measured placing the catheter tip at the APS nozzle level to define the initial conditions of the discrete phase in the numerical model. Even though the particle concentration in this point is not the optimal most of the particles were classified in the first and second event, which measures the particles between 0-20 µm.

The aerosolization rate (AR) has been measured for both compounds according to (2). The liquid chamber was filled up and the time needed to nebulize all the liquid was controlled with a chronometer.

$$AR = \frac{(m_{cam})_t - (m_{cam})_0}{t_{pulse} \cdot \rho} \tag{2}$$

where 0 is the instant before and t the instant after the nebulization pulse, m_{cam} is the mass of the liquid chamber, t_{pulse} is the time of the nebulization pulse and ρ is the density of the sterile water.

For a driving pressure of 4 bar, the AR corresponds to 1.98 ml/min for the sterile water and 1.06 ml/min for the FC-75. The rate of liquid nebulized increased proportionally with the increase of the driving pressure.

IV. NUMERICAL MODEL

The widespread availability of engineering workstations together with efficient solution algorithms and sophisticated pre- and post-processing methods enable the use of Computational Fluid Dynamics (CFD) techniques as a powerful tool to study and simulate the behavior of multiphase flows. In the work presented in this study the commercial CFD code Star CCM+ version 11.06 (CD Adapco®) [30] was used to create and run the numerical model.

A. Computational domain and boundary conditions

The problem was simplified making an axisymmetrical assumption to define the computational domain in order to save computational time in the simulation of the discrete particles. In this case, the six outer lumens are replaced by a ring, as shown in Fig. 4. The position of the air lumen (b_{lcen}) was maintained and the width of the ring was calculated by (3-5) in order to have the same area of the six outer lumens and consequently, the same air mass flow.

$$Original\ total\ outer\ lumen\ area = \frac{\pi \cdot d^2}{4} \cdot 6 \tag{3}$$

where d is the diameter of each of the six outer lumens in the distal tip, which is 66.4 µm for all of them.

$$Ring\ \ Area = 6 \cdot Outer\ Lumen\ Area \tag{4}$$

$$\frac{\pi \cdot (b_{lcen} + x)^2}{4} - \frac{\pi \cdot (b_{lcen} - x)^2}{4} = \frac{\pi \cdot d^2}{4} \cdot 6 \tag{5}$$

where x, which is the width of the ring, has a value of 23.36 µm.

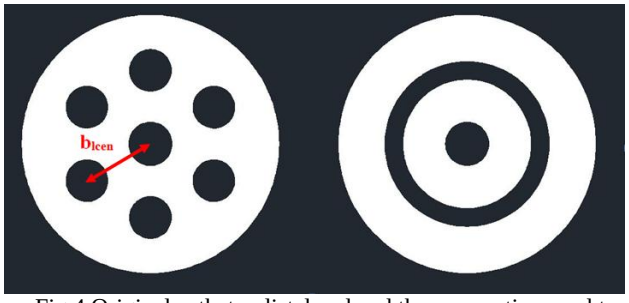

Fig.4 Original catheter distal end and the assumption used to create the axisymmetrical domain

The computational domain consists of the last 2 mm of the catheter and the downstream region beyond the catheter tip, as illustrated in Fig. 5. The outlet is located 52 mm away from the catheter tip, which is the optimal distance used for the experimental measurement of the FC-75 particle size distribution with the APS.

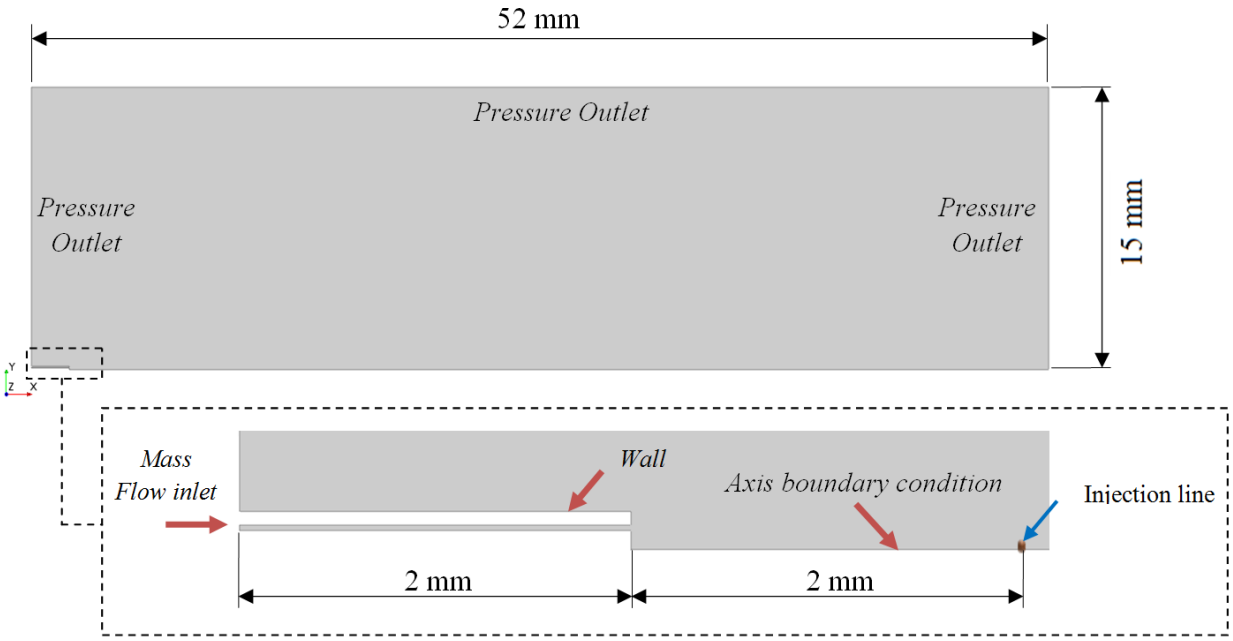

Fig. 5 Computational domain and boundary conditions

An air mass flow rate of 1.1344×10^{-5} kg/s, measured in a previous work with a driving pressure of 4 bar [20], was defined as the inlet boundary condition along with a temperature of 293K and a turbulence intensity of 0.07. An atmospheric outlet boundary condition was fixed for downstream boundaries and the axisymmetrical condition was set to the central axis. Ten particle injections were defined, as can be seen in Table VIII, to represent the particle size and mass distribution. The injection line was defined 2 mm away from the catheter tip as an estimated value between the APS nozzle and the laser beams which measures the distribution of the particles.

Injection	D_g (μm)	Mass flow rate (kg/s)
1	0.392	$3.41 \cdot 10^{-8}$
2	0.604	$2.68 \cdot 10^{-8}$
3	0.866	$3.17 \cdot 10^{-7}$
4	1.335	$2.41 \cdot 10^{-7}$
5	1.910	$6.88 \cdot 10^{-7}$
6	2.945	$1.20 \cdot 10^{-5}$
7	4.535	$6.31 \cdot 10^{-6}$
8	6.495	$1.55 \cdot 10^{-6}$
9	10.000	$1.61 \cdot 10^{-6}$
10	14.850	$4.90 \cdot 10^{-7}$

Table VIII. Particle initial conditions obtained from experimental measurements

B. Discretization

A mesh is the discretized representation of the computational domain, which the physics solvers use to provide a numerical solution. The computational domain was meshed by means of polygonal cells with a refinement defined along the central axis and near the distal tip of the catheter (See Fig. 6).

CFD results are strongly dependent on the mesh. Thus, a mesh dependency study based on Richardson's extrapolation was necessary to be performed [31]. A coarse, medium and fine meshes were defined with corresponding mesh sizes h_3, h_2 and h_1. A mesh refinement ratio of two was considered (6).

$$Mesh\ refinement\ ratio = r = \frac{h_2}{h_1} \tag{6}$$

The value used to do the study was the axial velocity at the end of the computational domain.

Mesh	Number of cells	V_{axial} (m/s)
M1	376.375	8.12
M2	182.418	7.98
M3	91.953	7.56

Table IX. Number of cells and axial velocity values at the end of the domain for each different mesh size

The extrapolated axial velocity value was calculated by means of (7) for h =0

$$\left(v_{axial}\right)_{h=0} = \left(v_{axial}\right)_1 + \frac{\left(v_{axial}\right)_1 - \left(v_{axial}\right)_2}{r^p - 1} \tag{7}$$

where *p* is the order of accuracy defined as (8)

$$p = \frac{\ln\left(\frac{\left(v_{axial}\right)_3 - \left(v_{axial}\right)_2}{\left(v_{axial}\right)_2 - \left(v_{axial}\right)_1}\right)}{\ln 2} \tag{8}$$

The grid convergence index (GCI) was also calculated. It is important that each mesh level yield solutions that are in the asymptotic range of convergence for the computed solution. This can be checked observing two GCI values as computed over three meshes (9-10). A small value of GCI indicates that the computation is within the asymptotic range [32].

$$GCI_{12} = F_s \frac{\left|\left(v_{axial}\right)_1 - \frac{\left(v_{axial}\right)_2}{\left(v_{axial}\right)_1}\right|}{r^p - 1} \cdot 100$$
$$GCI_{23} = F_s \frac{\left|\left(v_{axial}\right)_2 - \frac{\left(v_{axial}\right)_3}{\left(v_{axial}\right)_2}\right|}{r^p - 1} \cdot 100 \tag{9}$$

$$\frac{GCI_{23}}{r^p \cdot GCI_{12}} \approx 1 \tag{10}$$

	V_{axial} (m/s)	Error (%)
$(V_{axial})_{h=0}$ (m/s)	8.18	
M1	8.12	0.75
M2	7.98	2.39
M3	7.56	7.56

Table X. Error between the extrapolated value and the axial velocity for each mesh level

	Domain
GCI_{12} (%)	0.97
GCI_{23} (%)	3.23
GCI_{23}/r^pGCI_{12} (-)	**1.05**

Table XI. Grid Convergence Index results

Considering the relative error on each mesh level (See Table X) and that the relation GCI_{23}/r^pGCI_{12} is very close to 1 (See Table XI) the fine mesh (M1) with 376.375 was selected to develop the numerical model.

Due to the unsteady condition of the aerosol flow a temporal discretization is also necessary. A time-step of $1 \cdot 10^{-4}$ seconds was defined with 300 inner iterations per time-step to achieve the convergence of the numerical solution.

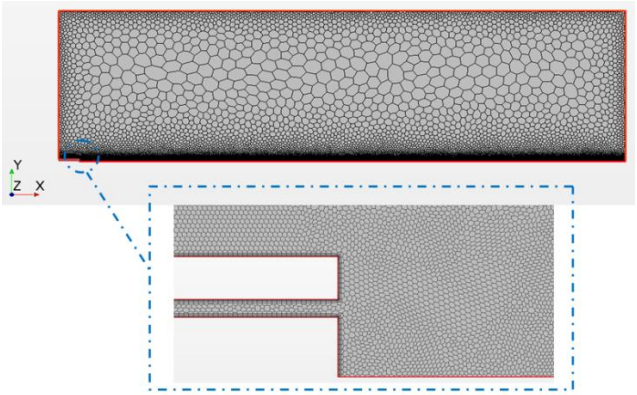

Fig. 6 Discretized representation of the computational domain

C. Physics and numerical models

CFD is based on the assumptions from continuum mechanics that the physics of fluid dynamics of any flow can be governed by three fundamental conservations: the conservation of mass, momentum and energy that form the Navier-Stokes equations of fluid flow. The turbulence models in CFD are responsible for providing closure of the governing equations in turbulent flows, i.e, when inertial forces are greater than viscous forces. In this study, the Realizable Two-Layer K-Epsilon model was selected to model the turbulent scales [33]. The discretized equations were solved by means of the Finite Volume Method. Due to the expected high air velocity at the tip of the catheter the Coupled flow solver was employed to solve the flow equations, which yields more robust and accurate solutions in compressible flows.

A Lagrangian reference frame was used to describe the evolution of individual particles as they traverse the domain. The framework is based on a Eulerian-Lagrangian approach where the conservation equations of mass, momentum and energy for the *dispersed phase* are written for each individual particle in Lagrangian form. This approach allows to calculate the trajectory of each individual particle. The governing equations for the *continuous phase* are expressed in Eulerian form and they are modified to take into account the presence of the dispersed phase. For flows involving a large number of dispersed particles, the total number of particles is represented by a smaller number of computational parcels. Each of these parcels represents a group of spherical particles that share the same properties. The Lagrangian tracking makes it easier to model a distribution of particle sizes of the dispersed phase which would have to be treated as separate phases using the Eulerian technique.

The Newton's second law of motion is solved for the dispersed liquid particles. The drag force, defined by (11), is the force acting on a single parcel due to the relative velocity between the particle and the continuous surrounding fluid in a uniform pressure field without relative acceleration.

$$F_D = \frac{1}{2} C_D \rho_C A_P |v_{rel}| v_{rel} \quad (11)$$

where C_D is the drag coefficient of the particle, ρ is the density of the continuous phase, v_{rel} is the relative velocity and A_p is the projected area of the particle. The drag coefficient used to calculate the drag force of a particle is defined using the Schiller-Naumann correlation [34]. Since the density of air is three orders of magnitude lower than the density of the dispersed particles, other forces such as the buoyancy force, the pressure gradient force and the virtual mass force were neglected. The gravity force was also considered negligible because of the high velocity values at the outlet of the catheter tip.

The turbulent dispersion that a particle in a turbulent flow experiences was modeled by the stochastic approach og Gosman and Ioannides [35] that includes the effect of instantaneous velocity fluctuations on the particle.

In a one-way coupled multiphase Eulerian-Lagrangian simulation the continuous phase is not influenced and fed back with information (source terms) from the dispersed phase. However, in cases with high speed, the coupling effect is too large to be neglected. A two-way coupling model was defined to simulate the interactions between the dispersed phase and the continuous phase. The volume fraction ϕ_c of all Lagrangian phases for which the two-way coupling is active is accumulated. This volume is seen as a void by the continuous phase: the volume available for the continuous phase decreases by this fraction (12).

$$\phi_C = \alpha\left(\sum \phi\right) + (1-\alpha)\cdot \phi_{C,old} \quad (12)$$

where α is the under-relaxation factor property of the two-way coupling solver.

After initialization of the particle injections the secondary breakup was modeled to predict the breakup of large particles into smaller particles due to high destructive forces. Collision and coalescence of the particles were not taken into account in this study. The CFD code provides a set of models that are used for the breakup of liquid droplets in a gaseous stream. A characteristic measure of this behavior is the Weber number defined by (13).

$$We = \frac{\rho_g |v_{rel}|^2 D_p}{\sigma} \quad (13)$$

Where ρ_g is the density of the continuous phase, v_{rel} is the relative velocity between phases, D_p is the particle diameter and σ is the surface tension of the discrete phase. The Taylor Analogy Breakup (TAB) was employed to simulate the breakup. The TAB model equations govern the droplet oscillation and distortion [36]. When the droplet oscillations reach the critical value y=1, defined in (14), breakup replaces the parent particles with child particles whose diameter is chosen from a Rosin-Rammler distribution.

$$y = \frac{2x}{C_b \cdot D_p} \quad (14)$$

where x is the instantaneous displacement of the droplet from its equilibrium position, C_b is an empirical constant and D_p is the particle diameter.

V. NUMERICAL SETUP AND EXPERIMENTAL VALIDATION

The continuity and Navier-Stokes equations are solved for the continuous phase (air) and the Newton's second law of motion is solved for the dispersed liquid droplets. Once the steady state air solution is converged the discrete phase was added by injection points defined within a line and simulated in transient state. A Courant number of 50 was used and a second-order upwind discretization scheme was selected for the conservation equations and turbulence. The source smoothing method was activated within the two-way coupling model; it uses a cell clustering technique to group together cells to form a coarser mesh on which to pass data. The size of the cluster is then independent of the underlying mesh size and is instead based on the size of parcels ensuring a smooth distribution of the source terms of the discrete particles in the continuous phase.

Continuous phase calculations were considered converged with a three-order-of-magnitude drop in numerical residuals, as shown in Fig. 7. Additionally, the axial velocity in a point at the outlet of the domain was monitored. The value change after the last 1000 iterations was $8.7 \cdot 10^{-3}$ %, confirming the convergence of the solution.

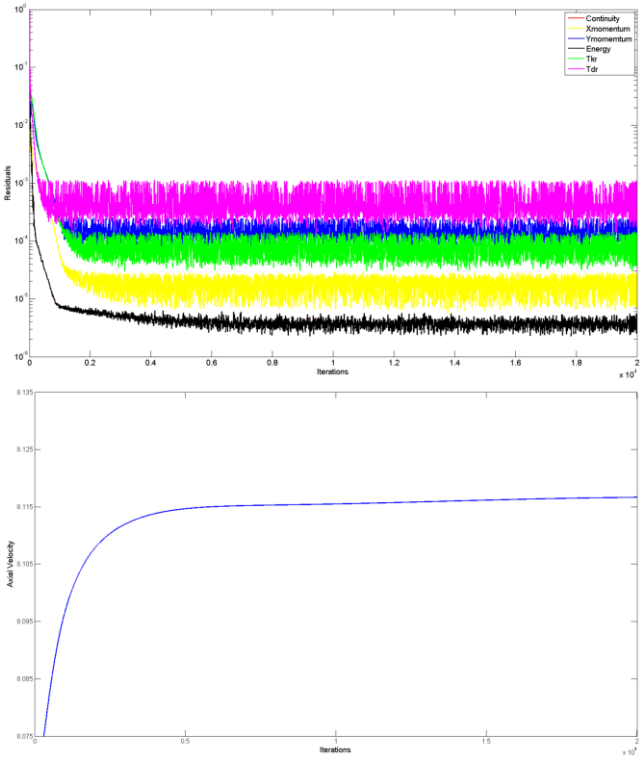

Fig.7 Residuals and axial air velocity values considered for the convergence of the numerical solution

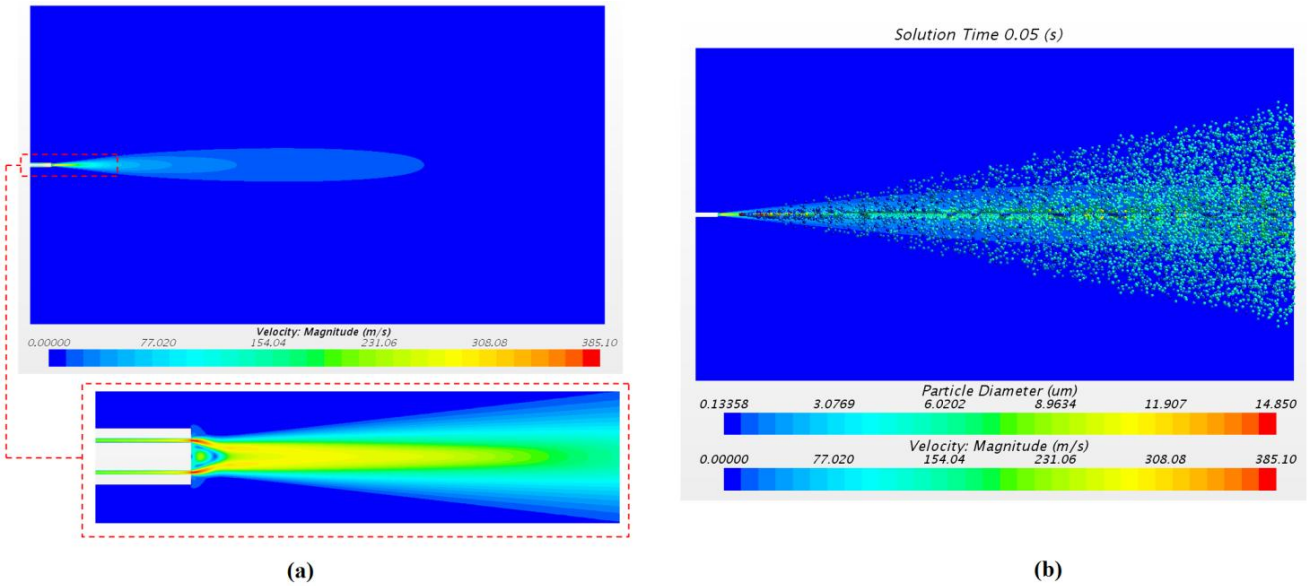

Fig. 8 Continuous phase velocity magnitude (a) and particle diameter of the discrete particles (b)

Fig. 8a illustrates the air flow velocity once the solution was converged The highest value was reached close to the outlet of the catheter tip with a peak of 385 m/s. The velocity value 2 mm away from the outlet, where the injectors were defines, was 238 m/s. This value was used subsequently as an initial condition to define the discrete phase injectors. These results confirm the necessity to consider the air as an ideal gas and to take into account the compressibility effects. Fig. 8b shows the numerical solution 0.05 seconds after the discrete phase was activated. Due to the transitory nature of the aerosol the particle distribution changes with time, therefore, it was necessary to track a representative sample of the solution to analyze the numerical results. A track of 0.01 seconds, corresponding to 100 time-steps was considered.

The axial velocity at different distances beyond the catheter tip were taken and validated with experimental data by means of a hot-wire constant temperature anemometer (Goikoetxea et al. [37]). The Realizable K-epsilon model used in the numerical model provide an accurate prediction of the air flow (See Fig.9).

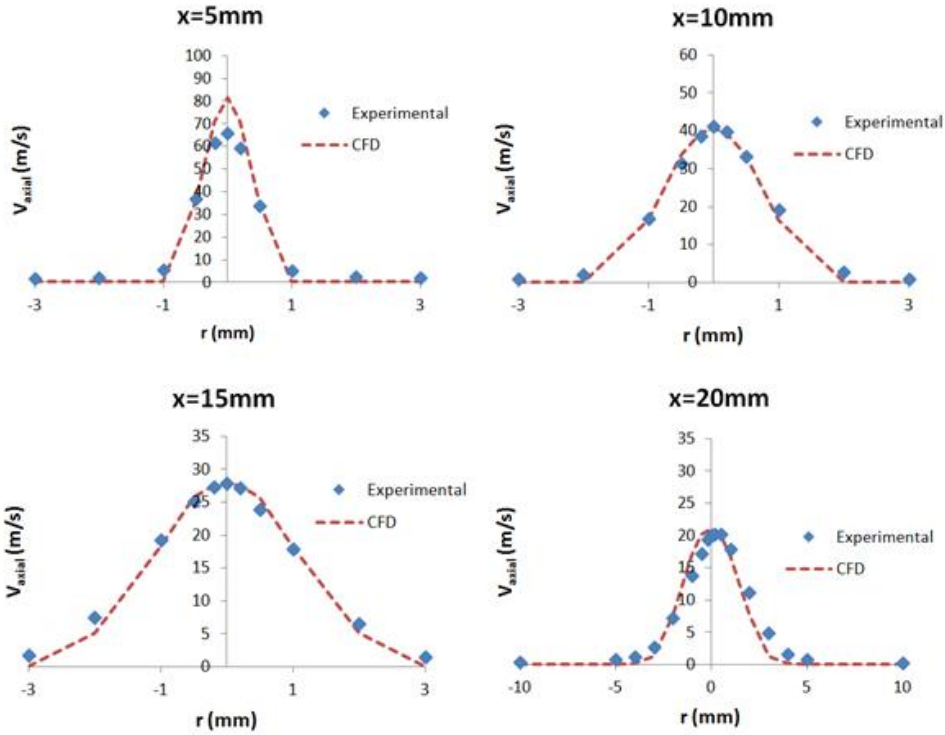

Fig.9 Experimental and numerical axial air velocity profiles at different distances from the catheter tip

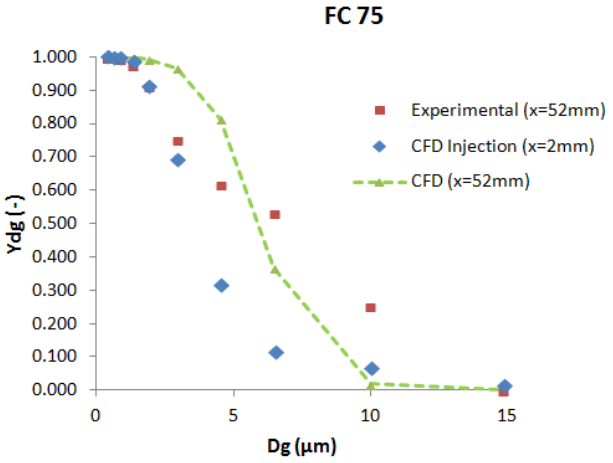

Fig. 10 Experimental and numerical cumulative mass distribution based on droplet size for the FC-75.

Numerical data were also obtained about the cumulative mass distribution in function of the droplet size (Y_{dg}) for the FC-75 aerosol. The results were compared with the previous experimental data measured with the APS and are illustrated in Fig. 10. The differences between the experimental and numerical solutions may be caused due to the collision and coalescence of the particles. In the numerical model, where the breakup of the particles was taken into account but not the collision and coalescence, the cumulative mass fraction was higher for particles below 5 µm and considerable lower for particles between 5 and 10 µm. This difference in the experimental validation of the particle mass distribution shows that the collision and coalescence of the particles plays a crucial role when it comes to define a numerical model of the aerosol generated by an inhalation catheter.

VI. Conclusions

The aerosol generated by an inhalation catheter (IC) has been studied by means of the Aerodynamic Particle Sizer (APS) along with CFD techniques. The GSD measured was between 1.89 and 2.19, resulting in heterodisperse aerosols. Note that the aerodynamic diameter (Da) was between the optimal recommended values (1-5 µm) and even though the MMAD is around 10 µm the study is focused to generate the aerosol beyond the nasopharyngeal area, avoiding the deposition of big particles.

Furthermore, a numerical model was created to study and simulate the aerosol generated with the compound FC-75. Experimental validation of the results confirmed the accuracy of the axial velocity profiles at different distances. The numerical results relative to the cumulative mass distribution of the particles and its experimental validation suggested the importance of the collision and coalescence of the aerosol particles.

Acknowledgment

Technical and human support provided by IZO-SGI, SGIker (UPV/EHU, MICINN, GV/EJ, ERDF and ESF) is gratefully acknowledged.

References

[1] B. D. Kamath, E. R. MacGuire, E. M. McClure, R. L. Goldenberg and A. H. Jobe, "Neonatal mortality from respiratory distress syndrome: Lessons for low-resource countries," *Pediatrics*, vol. 127, no. 6, pp. 1139-1146, 2011.

[2] A. H. Jobe and M. Ikegami, "Mechanisms initiating lung injury in the preterm," *Early Human Development*, vol. 53, no. 1, pp. 81-94, 1998.

[3] A. Bhandari and V. Bhandari, "Pitfalls, problems, and progress in bronchopulmonary dysplasia," *Pediatrics*, vol. 123, no. 6, pp. 1562-1573, 2009.

[4] E. Herting, "Less invasive surfactant administration (LISA) - Ways to deliver surfactant in spontaneously breathing infants," *Early Human Development*, vol. 89, no. 11, pp. 875-880, 2013.

[5] D. G. Sweet, V. Carnielli, G. Greisen, M. Hallman, E. Ozek, R. Plavka et al, "European consensus guidelines on the management of neonatal respiratory distress syndrome in preterm infants-2013 update, " *Neonatology*, vol. 103, no. 4, pp. 353-368, 2013.

[6] H. L. Halliday, W.O. Tarnow-Mordi, J. D. Corcoran and C. C. Patterson, "Multicenter randomized trial comparing high and low-dose surfactant regimens for the treatment of respiratory-distress syndrome (the curosurf-4 trial)," *Archives of Disease in Childhood*, vol. 69, no. 3, pp. 276-280, 1993.

[7] H. Verder, B. Robertson, G. Greisen, F. Ebbesen, P. Albertsen, K. Lundstrom et al, "Surfactant therapy and nasal continuous positive airway pressure for newborns with respiratory-distress syndrome," *The New England Journal of Medicine*, vol. 331, no. 16, pp. 1051-1055, 1994.

[8] F. Sandri et al, "Prophylactic or early selective surfactant combined with nCPAP in very preterm infants," *Pediatrics*, vol. 125, no .6, pp. E1402-E1409, 2010.

[9] P. A. Dargaville, A. Aiyappan, A. Cornelius, C. Williams and A. G. De Paoli, "Preliminary evaluation of a new technique of minimally invasive surfactant therapy," *Archives of Disease in Childhood -Fetal Neonatal Edition*, vol. 96, no. 4, pp. F243-F248, 2011.

[10] P. A. Dargaville, A. Aiyappan, A. G. De Paoli, C. A. Kuschel, C. O. F. Kamlin, J. B. Carlin et al. "Minimally-invasive surfactant therapy in preterm infants on continuous positive airway pressure," *Archives of Disease in Childhood -Fetal Neonatal Edition*, vol. 98, no. 2, pp. F122-F126, 2013.

[11] P. A. Dargaville, C. O. F. Kamlin, A. G. De Paoli, J. B. Carlin, F. Orsini, R. F. Soll et al. "The OPTIMIST-A trial: Evaluation of minimally-invasive surfactant therapy in preterm infants 25-28 weeks gestation," *BMC Pediatrics*, vol. 14, pp. 213, 2014.

[12] M. Arroe, L. Pedersen-Bjergaard, P. Albertsen, S. Bode, G. Greisen, F. Jonsbo et al. "Inhalation of aerosolized surfactant (exosurf (R)) to neonates treated with nasal continuous positive airway pressure," *Prenatal and Neonatal Medicine*, vol. 3, no. 3, pp. 346-352, 1998.

[13] G. Jorch, H. Hartl, B. Roth, A. Kribs, L. Gortner, T. Schaible et al. "Surfactant aerosol treatment of respiratory distress syndrome in spontaneously breathing premature infants," *Pediatric Pulmonology*, vol. 24, no. 3, pp. 222-224, 1997.

[14] E. Berggren, M. Liljedahl, B. Windbladh, B. Andreasson, T. Curstedt, B. Robertson et al. "Pilot study of nebulized surfactant therapy for neonatal respiratory distress syndrome," *Acta Paediatrica*, vol. 89, no. 4, pp. 460-464, 2000.

[15] N. N. Finer, T.A. Merritt, G. Bernstein, L. Job, J. Mazela and R. Segal, "An open label, pilot study of aerosurf (R) combined with nCPAP to prevent RDS in preterm neonates," *Journal of Aerosol Medicine and Pulmonary Drug Delivery*, vol. 23, no .5, pp. 303-309, 2010.

[16] J. J. Pillow and S. Minocchieri, "Innovation in surfactant therapy II: Surfactant administration by aerosolization," *Neonatology*, vol. 101, no. 4, pp. 337-344, 2012.

[17] W. Burkhardt, S. Kraft, M. Ochs, H. Proquitte, L. Mense and M. Rudiger "Persurf, a new method to improve surfactant delivery: A study in surfactant depleted rats," *PLoS One*, vol. 7, no. 10, pp. e47923, 2012.

[18] E. Koehler, G. Jilg, S. Avenarius and G. Jorch, "Lung deposition after inhalation with various nebulisers in preterm infants," *Archives of Disease in Childhood. -Fetal Neonatal Edition*, vol. 93, no. 4, pp. F275-F279, 2008.
[19] J. C. Dubus, L. Vecellio, M. De Monte, J. B. Fink, D. Grimbert, J. Montharu et al. "Aerosol deposition in neonatal ventilation," *Pediatric Research*, vol. 58, no. 1, pp. 10-14, 2005.
[20] E. Goikoetxea, X. Murgia, P. Serna-Grande, A. Valls-i-Soler, C. Rey-Santano, A. Rivas et al. "In vitro surfactant and perfluorocarbon aerosol deposition in a neonatal physical model of the upper conducting airways," *Plos One*, vol. 9, no. 9, pp. e106835, 2014.
[21] X. Murgia, E. Gastiasoro, V. Mielgo, F. J. Alvarez-Diaz, H. Lafuente, A. Valls-i-Soler et al, "Surfactant and perfluorocarbon aerosolization during different mechanical ventilation strategies by means of inhalation catheters: an in vitro study," *Journal of Aerosol Medicine and Pulmonary Drug Delivery*, vol. 25, no. 1, pp. 23-31, 2012.
[22] Z. H. Syedain, A. A. Naqwi, M. Dolovich and A. Somani, "In vitro evaluation of a device for intra-pulmonary aerosol generation and delivery," *Aerosol Science and Technol*ogy, vol. 49, no. 9, pp. 746-751, 2015.
[23] C. H. Zhang, Y. Liu, R. M. C. So and N. Phan-Thien, "The influence of inlet velocity profile on three-dimensional three-generation bifurcating flows," *Computational Mechanics*, vol. 29, no. 4, pp. 422-429, 2002.
[24] A. Farkas, I. Balashazy and K. Szocs, "Characterization of regional and local deposition of inhaled aerosol drugs in the respiratory system by computational fluid and particle dynamic methods," *Journal of Aerosol Medicine*, vol. 19, no. 3, pp. 329-343, 2006.
[25] P. Worth Longest, M. Hindle, S. Das Choudhuri and J.Xi, "Comparison of ambient and spray aerosol deposition in a standard induction port and more realistic mouth-throat geometry," *Journal of Aerosol Science*, vol. 39, no. 7, pp. 572-591, 2008
[26] Z. Liu, A. Li, X. Xu and R. Gao, "Computational fluid dynamics simulation of airflow patterns and particle deposition characteristics in children upper respiratory tracts," *Engineering Applications of Computational Fluid Mechanics*, vol. 6, no. 4, pp. 556-571, 2012.
[27] F.H.C. De Jongh, M. J. G. Rinkel and H. W. M. Hoeijmakers, "Aerosol deposition in the upper airways of a child," *Journal of Aerosol Medicine*, vol. 19, no. 3, pp. 279-289, 2006.
[28] E. Goikoetxea, A. Rivas, X. Murgia and R. Antón, "Mathematical modeling and numerical simulation of surfactant delivery within a physical model of the neonatal trachea for different aerosol characteristics," *Aerosol Science and Technology*, vol. 51, no. 2, pp. 168-177, 2017.
[29] X. Murgia, E. Gastiasoro, V. Mielgo, F. Alvarez-Diaz, H. Lafuente, A. Valls-i-Soler et al, "Surfactant and perfluorocarbon Aerosolization by means of inhalation catheters for the treatment of respiratory distress síndrome: an in vitro study," *Journal of Aerosol Medicine and Pulmonary Drug Delivery*, vol. 24, no. 2, pp. 81-87, 2011.
[30] CD Adapco version 11.06.011, http://mdx.plm.automation.siemens.com/
[31] L. F. Richardson and J. A. Gaunt, "The deferred approach to the limit. Part I. Single lattice. Part II. Interpenetrating lattices," *Philosophical Transactions of the Royal Society*, vol. 226, pp. 299-361, 1927.
[32] J. W. Slater, "Examining spatial (grid) convergence. NPARC alliance CFD verification and validation web site, National Aeronautics and Space Administration.
[33] D. C. Wilcox, *Turbulence Modeling for CFD*. La Cañada, CA: DCW Industries, Inc, 2006.
[34] L. Schiller, A. Naumann, "Ueber die grundlegenden Berechnungen bei der Schwerkraftaufbereitung," Ver. Deut. Ing. Vol. 77, pp. 318-320, 1933.
[35] A. D. Gosman and E. Ioannides, "Aspects of computer simulation of liquid-fueled combustors," *Journal of Energy*, vol. 7, no. 6, pp. 482-490.
[36] P. O'Rourke and A. Amsden, "The TAB method for numerical calculation of spray droplet breakup," SAE Technical Paper 872089, 1987.
[37] E. Goikoetxea, "Evaluación de una técnica de nebulización para la administración de surfactante en la población neonatal. Establecimiento de las pautas para el diseño de un nuevo dispositivo," Ph.D. dissertation, Tecnun-Engineering School, University of Navarra, San Sebastian, Spain, 2015.